Seasonal bedload pulses in a small alpine catchment

Frédéric Liébault, Jonathan Laronne, Sébastien Klotz, Coraline Bel

Seasonal bedload pulses in a small alpine catchment

Frédéric Liébault[1*], Jonathan B. Laronne[2], Sébastien Klotz[3], Coraline Bel[4,5]

[1] Université Grenoble Alpes, INRAE, ETNA, 38 000 Grenoble, France, frederic.liebault@inrae.fr

[2] Dept. of Geography & Environmental Development, Ben Gurion University of the Negev, Israel, john@bgu.ac.il

[3] Université Grenoble Alpes, INRAE, ETNA, 38 000 Grenoble, France, sebastien.klotz@inrae.fr

[4] Université Grenoble Alpes, INRAE, ETNA, 38 000 Grenoble, France

[5] Present address: EDF R&D, LNHE, Chatou, France, coraline.bel@edf.fr

* corresponding author

Highlights

- New field-based bedload monitoring datasets in a small alpine badland catchment
- Direct field observation of sediment pulse effect on bedload response to flow
- Counterclockwise seasonal hysteresis of bedload transport

Abstract

Natural fluctuations of bedload transport under steady hydraulic conditions have been often attributed to the propagation of sediment pulses in river channels, leading to hysteretic patterns in bedload rating curves at both the hydrograph and the seasonal timescales. However, direct field observations of the sediment pulse effect on bedload transport rates have been rarely reported. Two bedload datasets recorded in a small Mediterranean badland catchment of the Southern French Prealps (Moulin Ravine at Draix) are used here to investigate the effect of sediment pulses originating from hillslopes on the bedload response to flow conditions. The first dataset comes from a long-term erosion monitoring program providing time-integrated bedload yields since the late 1980s by means of a large sediment trap. The second dataset is based on a slot sampler providing bedload fluxes at a 1-min time resolution since autumn 2011. Sediment pulses have been tracked with regular scour chain surveys along the alluvial channel upstream of the bedload monitoring station. Both datasets revealed a seasonal counterclockwise bedload hysteresis which can be attributed to a yearly sediment pulse reaching the catchment outlet during autumn and early winter. We believe that these seasonal bedload pulses could be typical of small alpine catchments with active gully erosion on bedrock sensitive to frost-cracking processes.

Keywords

Bedload transport monitoring, bedload pulses, hysteresis, badlands

1. Introduction

Bedload transport in stream channels is prone to a very high level of temporal fluctuations, even under steady hydraulic conditions, making the prediction of fluvial bedload transport quite uncertain (Jackson and Beschta, 1982; Gomez and Church, 1989; Gomez et al, 1989; Whiting et al., 1999; Froehlich, 2003). These fluctuations have often been attributed to the effect of travelling sediment pulses, also referred as sediment waves, which can have different origins, and which can be observed at different spatiotemporal scales (Hoey, 1992; Nicholas et al., 1995; Lane et al., 1996; Aigner et al,

2017; Zapico et al., 2018). This is particularly true in upland environments, where the multiplicity of active sediment sources on hillslopes combined with the presence of massive alluvial storages within channel sedimentary units with different mobility generate a complex sediment cascading system (Warburton, 1992; Benda and Dunne, 1997; Fuller and Marden, 2010; Piton and Recking, 2017). Bedload transport can be affected by a sudden increase of sediment supply under the effect of bank erosion, bar destruction, or hillslope inputs (e.g. landslides, debris flows). In addition, experimental studies demonstrated that sediment release from autogenic channel scouring may also explain instantaneous fluctuations of bedload flux (Recking et al., 2009). At longer timescales, seasonal or annual shifts of bedload rating curves are also reported for a variety of fluvial environments (e.g., Nanson, 1974; Garcia et al., 2000; Hassan and Church, 2001; Lenzi et al., 2004; Ryan et al., 2005; Barzilai et al., 2013; Rickenmann, 2018; Comiti et al., 2019).

The variability of bedload transport during flow events has commonly been investigated by detecting and interpreting hysteretic patterns of bedload rating curves. The first field dataset documenting such patterns is very likely the Oak Creek bedload record in the Oregon Coast Range, showing a counterclockwise hysteresis at the event scale (Milhous, 1973; Klingeman and Emmett, 1982). Since this early publication, bedload hysteresis has been reported for a wide range of flow regimes (rainfall, snowmelt, and glacial-melt regimes), spatial scales (drainage basins from 1 to 600 km^2), and for timescales generally ranging from seasonal, daily, to hourly periods of time (and even shorter during flume experiments). Among these studies, a prevalence of daily (or event-based) clockwise hysteresis emerges, with higher bedload fluxes per unit discharge during rising limb of hydrographs (Table A.1). This has been attributed to (i) the release of loose sediment patches in the channel or along the banks, readily available for transport (Klingeman and Emmett, 1982; Sidle, 1988; Hassan and Church, 2001; Vatne et al., 2008; Mao et al., 2014; Krein et al 2016; Rickenmann, 2018), (ii) to antecedent active flow conditions having loosened the bed (Reid et al., 1985), (iii) to the lag in formation of roughness elements or bedforms (Kuhnle, 1992; Hsu et al, 2011; Roth et al., 2014), or (iv) to the increase of slope of the energy line during rising limbs (Meirovich et al., 1998; Schneider et al., 2016). Daily counterclockwise patterns have also been described and related to (i) armour breaking (Milhous, 1973;

Sidle, 1988; Krein et al, 2016), (ii) long antecedent periods of low flows having consolidated the bed (Reid et al., 1985), (iii) sediment release from distant sediment sources, like glacial zones (Mao et al., 2014) or upper river reaches with gravel storages (Aigner et al., 2017). Seasonal hysteresis loops are less common in the literature (Table A.1), but both clockwise and counterclockwise patterns have been reported. Clockwise seasonal patterns were documented as early as 1974 during the snowmelt flow season of a small mountain stream in the Rocky Mountains (Nanson, 1974). The decrease of bedload concentration over the high-flow season was attributed to the sediment flushing effect of the spring peak flow, which remobilizes loose sediment deposits that accumulated in the channel and along the banks during the preceding freeze-thaw season. This bedload transport response has also been observed in snowmelt mountain streams of Idaho (Moog and Whiting, 1998) and in the French Alps (Misset et al., 2020), in two small proglacial streams of Alaska (Pearce et al., 2003), as well as in a mountain stream in China under temperate pluvial regime (Yu et al., 2009). The latter study introduces the notion of travelling bedload masses that generate seasonal sediment pulses. Activation of specific sediment sources has also been invoked to explain seasonal clockwise hysteresis in glacier-fed mountain streams in Switzerland and Austria (Schneider et al., 2016; Rickenmann, 2018). The only known case of counterclockwise seasonal hysteresis is likely the Saldur River in the Eastern Italian Alps, where the pattern has been attributed to sediment pulses originating in glacial zones and reaching the bedload monitoring station during the late summer runoff season (Comiti et al., 2019). Several flume datasets also provide experimental evidence of the effect of bedform migration (Gomez et al., 1989), antecedent hydrological conditions (Monteith and Pender, 2005; Mao, 2018), or temporal lag (Phillips and Sutherland, 1990) on bedload hysteresis.

Although sediment pulses have often been presented as a cause of seasonal hysteresis of bedload transport, coincident observations of bedload flux and travelling sediment pulses at the seasonal scale are still lacking to provide direct evidence of this effect. More specifically, evidence of the recurrence of hysteretic bedload response to water discharge coincident with observations of channel sediment storage change is lacking. With this in mind, we investigated seasonal fluctuations of bedload transport in a small Mediterranean badland catchment of the Southern French Alps by monitoring the

occurrence of bedload pulses as well as the concomittant scour and fill of upstream reaches. Our objective is to present the seasonal pattern of bedload response to flow documented by two complementary bedload monitoring datasets of high and low time frequency records, and to determine the effect of travelling sediment pulses on this pattern. This allows determining the role of sediment pulses travelling through the stream network and the temporal variability of bedload response.

2. Study site

The Moulin Ravine drains an 8.9 ha Mediterranean catchment entrenched in Jurassic black marls of the Southern Prealps, in SE France near Digne-les-Bains (midpoint at 44°08'32''N, 6°21'42''E - Fig. 1). The mean elevation of the catchment is ~900 m asl. The catchment is part of the long-term erosion observatory of Draix in Haute-Provence, which has been operating since the early 1980s in a set of experimental catchments with contrasted size and forest cover (Mathys et al., 2003). Alpine black marls, a consolidated mudstone, are prone to active gullying erosion, resulting in a typical badland relief eroding at a rate of ~1 cm yr^{-1} at Draix (Mathys, 2006). The mean annual rainfall is ~900 mm, with largest flow events in the ravines generally occurring during late spring and summer convective storms, and occasionally during autumn Mediterranean episodes. The seasonal distribution of rainfall is typical of a Mediterranean climate, with one major peak in autumn and a secondary peak during spring. The mean daily temperature measured since 2000 at the Draix observatory meteorological station is 10.3 °C, with a maximum in August, and minimum negative daily temperatures regularly occurring from December to March (Mathys, 2006). The production of loose debris on marly hillslopes is controlled by the temperature regime, as recently documented by Ariagno et al. (in press) establishing that the yearly sediment export of Draix badlands is modulated by cold-season frost-weathering processes, approximated by the time spent below 0 °C and by a frost-cracking intensity indicator. Detailed descriptions of the Moulin catchment are summarized in Liébault et al. (2016) and Jantzi et al. (2017).

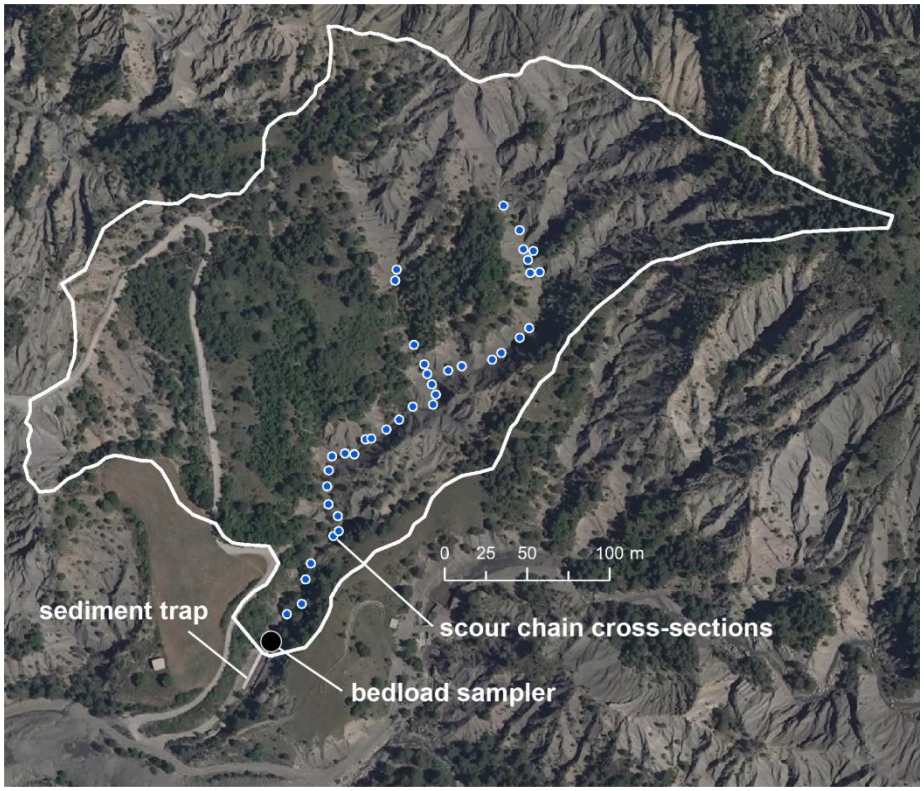

Figure 1. Bedload monitoring equipment of the Moulin experimental catchment at Draix; the white line represents the catchment divide; 2009 ortho-imagery from IGN France.

Despite its small catchment size, the Moulin is characterized by the presence of a well-developed alluvial system operating as a buffering zone between sediment sources from active hillslopes and the catchment outlet, thereby regulating the highly fluctuating sediment supply from hillslopes. This confined alluvial system features typical fluvial forms such as miniature braided channels and alluvial terraces. The mean channel slope is 0.045, and the mean active channel width is ~2.7 m. Particularly interesting is the seasonal pattern of changing channel conditions observed along the main channel (Fig. 2), as documented using qualitative photo surveys (Mathys, 2006). The typical channel condition that progressively emerges in spring and summer is a flat (low relative relief) braided channel overloaded with fine-grained ($D_{50} \approx 2$ mm) sediment (Liébault et al., 2016). This fluvial landform is the consequence of a transport-limited sediment regime induced by a high sediment supply from hillslopes, under the cumulative effect of loose debris accumulation on hillslopes during winter, and the occurrence of high-intensity convective storms during spring and summer, generating sediment pulses from hillslopes. In late summer and autumn, conditions progressively shift to a supply-limited

144 regime, under the effect of sediment exhaustion from hillslopes. This has been explained by the
145 flushing of the easily available loose debris during antecedent storms, and by the autumn rainfall
146 regime, characterized by lower intensity and longer duration rainfall events (Liébault, 2017). This
147 contributes to the formation of a narrow and coarse-grained channel entrenched into remnant terraces
148 of the previous summer. The incision may locally lead to outcropping of bedrock.

149

150 Figure 2. Seasonal shifting channel conditions of the Moulin Ravine. In spring and summer (A), an
151 aggrading channel overloaded with fine-grained bedload sediment is forming; in autumn (B), channel
152 incision occurs, with the formation of an entrenched rough bed with alluvial terraces and bedrock
153 outcrops (©F. Liébault).

154

155 ## 3. Materials and methods

156 ### 3.1. Bedload monitoring with the sediment trap

157 Bedload transport by the Moulin is monitored since April 1988 by means of a 150 m^3 sediment trap
158 deployed at the catchment outlet (Fig. 3A). The trap is a rectangular concrete retention basin closed by
159 a grill-slit check-dam, specifically designed to fully capture the coarse fraction of the sediment
160 transport. Regular topographic surveys provide a time-integrated continuous record of sediment
161 deposition in the trap since 1988. These surveys are undertaken with a total station after each flow
162 event, provided that the time between two successive events is long enough to collect the data. The
163 uncertainty in the volume of sediment deposition based on topographic differencing was estimated at
164 ~1 m^3 (Mathys, 2006). Once the trap is full of sediment, its full retention capacity is restored by a

mechanical dredging operation. Bedload volumes obtained from the sediment trap are to be regarded as higher-bound estimates of the true bedload yield due to integration of fine sediment settling not merely in the distal part of the trap, but also in the proximal zone; in this environment fines are present in the active bedload layer (Liébault et al., 2016). Grain-size distributions (GSDs) of bulk sediment samples obtained from the trap revealed that the fraction < 0.063 mm (silts and clays) can represent 13 - 27% of the mass (Fig. A.1). Only few GSD curves of trap deposits are available, hence we have not attempted a systematic correction of bedload yields. We assume that the fine fraction included in bedload yields did not substantially change through time.

Figure 3. The 150 m^3 sediment trap (A), and the Reid (or Birkbeck) bedload slot sampler (B) used for low and high frequency bedload monitoring of the Moulin Ravine, respectively; an example of scour chain used for monitoring scour and fill processes in the Moulin channel is presented in panel C (©F. Liébault).

We investigated the bedload rating curve of the Moulin based on 230 sediment trap surveys undertaken between November 1990 and October 2019, representing 80% of the entire deposition dataset. Though surveys were undertaken prior to November 1990, hydrological monitoring of the

Moulin started 2.5 years after trap deployment, hence our starting date is 1990. During the period between November 1990 and October 2019, a total of 56 dredging operations were undertaken to maintain the retention capacity of the trap, on average about 2 dredgings per year. Altogether 58 surveys after November 1990 were excluded from the analysis mainly due to gaps in the hydrological time series, and secondarily to partial deposition records related to the exceedance of the trap retention capacity, or to unrealistic bedload volumes (V_b) compared to runoff volumes over the period of bedload transport (R). Bedload concentration by volume (C_b) was computed as:

$$C_b = V_b (1-p) / R \quad (1)$$

with p, the sediment porosity. A constant 1700 kg m^{-3} bulk sediment density was considered, equivalent to a sediment porosity of 0.36. This value was measured in the sediment trap of the neighboring Laval catchment and is systematically used at Draix for volume-mass conversions of sediment deposits (Mathys, 2006). The period of bedload transport was extracted considering a critical discharge for bedload transport of 11.2 L s^{-1}. This corresponds to the lowest peak water discharge associated with bedload entry into the trap. A bedload concentration threshold of 0.16 was considered for filtering unrealistic bedload volumes. This threshold was derived from the maximum suspended sediment concentration (ca. 420 g L^{-1}) observed at the Moulin (Mathys et al., 2003). Considering that bedload comprises about half of the total sediment load of the Moulin (Mathys, 2006), the maximum bedload concentration by volume is ≈ 0.16. Excess runoff volumes (E_R) were also computed by time-integration of water discharges above the critical discharge of bedload transport. It is acknowledged that the critical discharge is not steady over the monitoring period, since it is influenced by changing channel conditions. Our approach computing excess runoff volume is conservative, especially for spring and summer flow events, for which a higher critical discharge, and a subsequently higher bedload concentration is expected. Therefore, the effect of increasing the critical discharge by a factor of two for spring and summer flow events was tested to determine if this has a strong effect on seasonal bedload responses to flow.

For each period between two selected sediment trap surveys, the water discharge time series of the Moulin was used to extract hydrological predictors for bedload transport (Fig. 4). The two considered

predictors are the instantaneous peak discharge recorded during the period between two sediment trap surveys (Q_{max}), and the total excess runoff volume (E_R) during the same period. Water discharge monitoring at the Moulin is based on two complementary gauging stations. One station is equipped with a Parshall flume and provides water discharge for small flow events; another station is equipped with a trapezoidal flume providing water discharge for the largest flow events during which the Parshall flume is overflooded. A detailed description of the hydrological monitoring is available in Mathys (2006), who estimated an uncertainty of less than 10% for low discharges, and about 10% for high discharges.

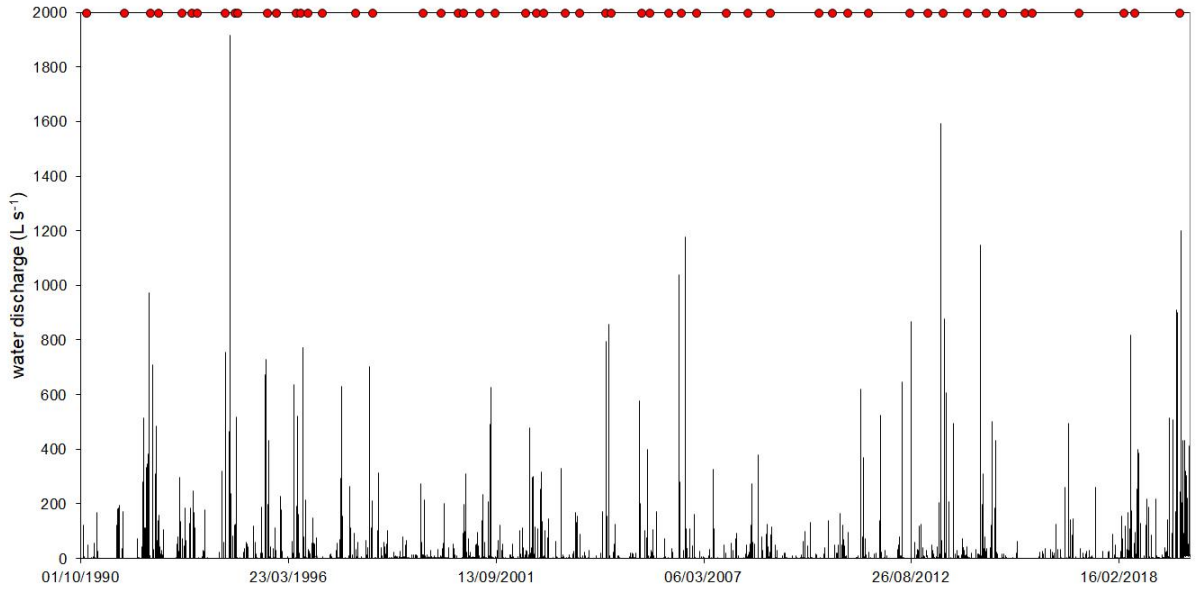

Figure 4. The hydrological time series of the Moulin between October 1990 and December 2019, with dates of the 56 sediment trap dredgings during the period (red points).

3.2. Bedload monitoring with the slot sampler

A high-frequency bedload monitoring program at the Moulin started in autumn 2011 to investigate the bedload response to flow, using a Reid (previously termed Birkbeck) slot sampler deployed at the exit of the catchment. Bedload monitoring has been maintained by a regular maintenance of the sampler during more than 6 years (until March 2018). This automatic sampler has been recognized as the most reliable apparatus for the direct unmanned sampling of bedload during floods, since it is a very efficient tool to separate bedload from suspended load (Poreh et al., 1970; Reid et al., 1980; Laronne

et al., 2003). The sampler operates as a device which continuously weighs the mass of bedload accumulating in a bed excavation after having fallen into a slot flush with the bed. Sediment is deposited in a box positioned over a water-filled pressure pillow connected to a vented pressure transducer. A second independent vented pressure transducer records the hydrostatic pressure, thus allows isolating the pressure response associated with bedload deposition in the box from the hydrostatic pressure.

The Moulin slot sampler was deployed about 10 m upstream from the sediment trap, at the head of a straight embanked trapezoidal channel (Fig. 3B). The approach reach of the sampler is a hillslope-confined alluvial channel with a riffle-pool-bar morphology, characterized by a mean channel slope of 0.045, a mean bankfull width and depth of 2.7 and 0.5 m, respectively, and a mean surface D_{50} of 2 mm. A concrete weir was constructed across the entire channel reach from the sampler downstream to ensure that the slot is always flush with the bed. The sampler provides specific (per unit width) bedload fluxes for 10 s time increments during flow events, as long as the inner box of the sampler is not full of sediment. The full capacity of the Moulin sampler (0.34 m^3) was most of the time insufficient to store the total bedload mass passing through the slot width during a flow event, as is typical of bedload monitoring with slot samplers. However, the sampler allowed exploring a wide range of flow conditions distributed through different seasons. The regular operation of the sampler since late 2011 allows us to fulfill this objective and to investigate the seasonal bedload responses of the Moulin. The precision of the two transducers used in the sampler for the monitoring of the pressure differencing gives a mass resolution of 1.33 kg (95% confidence interval). To integrate periods with low bedload fluxes in the present dataset, a constant time increment of 60 s has been used to compute unit bedload flux. A systematic grain-size analysis of the sampled sediment mass was used to remove the fraction below 0.063 mm for computing bedload mass. This fine-grained fraction is higher than expected with slot samplers, as it generally represents 15 - 20% of the sampled mass in the Moulin. This is explained by the very high suspended sediment concentrations encountered in the marly badlands of Draix, commonly several hundreds g L^{-1} in the Moulin, notably during summer convective storms (Mathys et al., 2003). The proportion of fines in the Moulin active bedload layer is equivalent

to the one observed in the sampler, suggesting that fine-grained particles enter the slot embedded with coarse particles (Liébault et al., 2016). A full technical description of the slot sampler with illustrations as well as the calibration and data processing protocol are provided in previous papers (Liébault et al., 2016 and 2017).

The initial slot width of the bedload sampler was 4 cm; it was increased to 8 cm after constraining bedload motion by lateral vanes deployed in April 2013. The deployment of lateral vanes was required due to lateral bedload inputs during the first year of monitoring, which led to unrealistic unit bedload flux estimations. For these early monitored events, a sampling width equal to the slot length (50 cm) was used for computing unit bedload flux. This is justified by our observations during flow events, revealing oblique flow directions with respect to the slot width, and therefore possibility for bedload particles to enter the sampler from the entire length of the slot.

The high-frequency bedload rating curve has been obtained by considering the channel-average shear stress (τ in N m^{-2}) associated with 60 s bedload fluxes, computed as:

$$\tau = \rho g R s \quad (2)$$

with ρ the fluid density calculated by considering the suspended sediment concentration monitored at the Moulin using an ISCO sampler (see Liébault et al., 2016 for details), g the constant of gravitation, R the hydraulic radius computed for the cross-section at the sampler (using flow depths recorded by the sampler's pressure transducer, and a constant bed width of 1.4 m), and s the slope of the energy gradient, which was assumed to be equal to the streambed slope (assumption of steady and uniform flow regime). The channel slope was not considered to be temporally constant, but computed for each flow event by considering net elevation changes at the first scour chain section upstream of the sampler (see section 3.3). The channel slope prior to each flow event was used for computation of average cross-sectional shear stress.

3.3. Scour chain surveys

The alluvial storage of the main branches of the Moulin Ravine were surveyed since the summer of 2007 using a set of ~80 stainless steel scour chains deployed along 39 cross-sections (Fig. 1). Scour chains are used to record for each sampling point the maximum depth of scour and the net deposition since the last survey (Leopold et al., 1966; Liébault and Laronne, 2008). The main advantage of scour chains compared to classic repetitive topographic surveys is that they detect scour and fill compensations.

Scour chains have been deployed along the main branches of the stream network where significant cut-and-fill processes are regularly observed (Fig. 3C). This includes a ~500 m total stream length. One to three scour chains at each cross-section were inserted down to bedrock. Scour-and-fill depths have been systematically collected since September 2007, with the purpose of producing an event-based survey, but the time between two flow events was at times too short to collect the data in between.

Scour chain data have been used to document altimetric changes of the Moulin channel during the period of bedload monitoring with the slot sampler (since spring 2011). This includes 45 scour chain surveys for which the net volumetric change of the alluvial storage was computed using the entire set of recovered active scour chains. Summary information about the scour-chain surveys used in this study is provided as supplementary material (Table A.2). The initial alluvial storage at the onset of monitoring was assed using detailed surveys of the thickness of alluvial cover by manual probing down to the bedrock (see Jantzi et al., 2017 for more details). A scour chain was considered active if it recorded a scour or fill activity during the surveyed period. Confidence intervals of erosion and deposition volumes for each scour-chain survey have been obtained from standard errors of mean scour and fill depths. It was then possible to separate recorded bedload fluxes into three different phases of channel evolution : (i) aggradation when a significant increase of the alluvial storage volume was observed, (ii) degradation when this volume significantly decreased, and (iii) equilibrium when this volume was stable. The recovery rate of scour chains fluctuated between 83% and 100%, and the proportion of active scour chains ranged from 8 to 90%. To obtain a stable temporal density of

observations, we regularly replaced lost scour chains, generally during winter when the alluvial cover was thin, facilitating the anchoring of the chain to the bedrock.

4. Results

4.1. Time-integrated bedload volumes

Selected sediment trap surveys undertaken during the past 29 years (n=230) reveal that both peak discharge and total excess runoff volume are relatively good hydrological predictors of time-integrated bedload volumes. Results from linear regressions on log-transformed values show a R^2 of 0.54 (p<0.0001) for peak discharge (V_b=0.278$Q_{max}^{0.74}$), and a R^2 of 0.53 (p<0.0001) for excess runoff volume (V_b=0.584$E_R^{0.48}$). A strong data scatter is however observed with both predictors, with bedload volumes typically fluctuating over one order of magnitude for a given peak discharge or excess runoff volume. Following the approach proposed for the Erlenbach (Rickenmann, 1997), a slightly improved multiple regression was obtained with log-transformed values for both hydrologic predictors (R^2 = 0.64; V_b=0.212$Q_{max}^{0.45}E_R^{0.28}$). Coefficients show a stronger effect of the peak discharge. This dataset also shows that power laws offer much better fits to the data than linear regressions (R^2 = 0.29 and 0.30 for peak discharge and excess runoff volume, respectively). If the critical discharge for bedload transport is increased by a factor of 2 for spring and summer, 15 surveys are excluded from the database, and linear regressions on log-transformed values show lower R^2 values for both peak discharge (0.48) and excess runoff volumes (0.46).

Sediment trap surveys were classified by season, considering a binary clustering into cold (autumn and winter) and warm (spring and summer) seasons. This classification was used to study the seasonal evolution of bedload rating curves. Sediment trap surveys associated with peak discharge occurring between early September and end of March were grouped into the cold seasons, while the warm seasons were considered between early April and end of August. This criterion for seasonal classification was the most differentiating in terms of bedload rating curves. This analysis shows that power laws with peak discharge offer the best fits for the two groups (R^2 of 0.62 and 0.47 for warm and cold seasons, respectively, versus R^2 of 0.45 and 0.17 with linear regressions), with similar

exponents ca. 0.75, but with a higher intercept for the autumn-winter group (Fig. 5). Despite a strong data scattering for the two groups, constant terms of linear regressions on log-transformed values show a 52% increase of the mean bedload transport during cold seasons (Table 1). A covariance analysis (ANCOVA) was undertaken to compare the two regression models by testing the effect of the season (binary categorical factor) on bedload rating curves. Results show a very significant difference of intercepts (F= 15.130; p<0.001), and similar regression slopes (F=0.003; p=0.95). A complementary ANCOVA performed with the reduced sample of spring and summer surveys resulting from a 2-fold increase of critical discharge show a significant difference of intercepts between groups (F=12.998; p<0.001). Another test for seasonal effect was performed using an integrated hydrologic predictor H_P, derived from the multiple regression analysis considering the cumulative effect of peak discharge and effective runoff volume on bedload transport ($H_P=Q_{max}^{0.45}E_R^{0.28}$). Although the integration of effective runoff reduces the seasonal shift of bedload response, the intercept of the autumn-winter group is significantly higher, as shown by ANCOVA result based on H_P (F=5.039, p=0.0257). The seasonal effect on bedload transport is statistically confirmed, but the rate of bedload transport increase with water discharge does not change between seasons. When the four seasons are considered separately, the most important shift is observed between autumn and spring, as shown by constant terms of log-linear regressions (Table 1). Although power law regressions can be successfully fitted with peak water discharges for each season, the quality of the regression is lower for the winter dataset, likely because the number of events is lower (n=22) than for the other seasons.

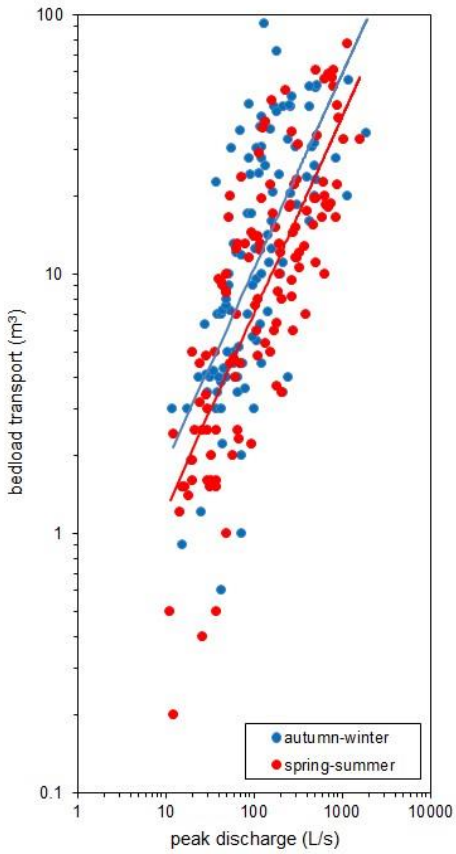

359

360 Figure 5. Seasonal bedload rating curves of the Moulin obtained from sediment trap surveys between
361 October 1990 and December 2019; best fits obtained with a power-law (V_b=0.329$Q_{max}^{0.75}$ for autumn-
362 winter, V_b=0.216$Q_{max}^{0.76}$ for spring-summer, with V_b the time-integrated bedload volume (m^3), and
363 Q_{max} the peak water discharge (L s^{-1}).

364

	Autumn-Winter	Spring-Summer	Autumn	Winter	Summer	Spring
Best fit	V_b=0.329$Q_{max}^{0.75}$	V_b=0.216$Q_{max}^{0.76}$	V_b=0.320$Q_{max}^{0.75}$	V_b=0.160$Q_{max}^{0.95}$	V_b=0.240$Q_{max}^{0.73}$	V_b=0.144$Q_{max}^{0.87}$
R^2	0.47	0.62	0.51	0.31	0.57	0.56
F Fisher	94.1	197.9	87.4	9.0	95.5	61.1
p-value	<0.0001	<0.0001	<0.0001	0.007	<0.0001	<0.0001
N	107	123	85	22	74	49
Constant term*	0.158-0.685	0.127-0.368	0.146-0.700	0.010-2.676	0.106-0.542	0.057-0.367
Exponent*	0.60-0.90	0.65-0.86	0.59-0.91	0.29-1.61	0.58-0.88	0.64-1.09

365 *(95% CI)

366 Table 1. Summary statistics of linear regressions on log-transformed values of time-integrated bedload
367 volume *vs* peak water discharge using data from sediment trap surveys between November 1990 and
368 October 2019; V_b: bedload transport volume (m^3); Q_{max}: peak water discharge (L s^{-1}).

369

Seasonal patterns of bedload transport have also been scrutinized through data processing at a monthly time resolution for the 1990-2019 period. Monthly peak water discharges were systematically extracted from the full hydrological time series to characterize the seasonal pattern of hydrological forcing. This reveals that the highest peak discharges are concentrated during the warm seasons (spring-summer), with an extended period of intensive runoff between June and September (Fig. 6B). Flood runoff starts declining in October and reaches a minimum between January and March, as shown by mean values of peak water discharge. The monthly pattern of bedload transport volumes obtained from sediment trap surveys (including all bedload yields that can be unequivocally assigned to a month, n=252) shows a similar increase during spring with a peak reached in early summer, but conversely to flood runoff, bedload transport remains at a peak level until early winter (Fig. 6A). A sigmoid curve describes this seasonal pattern of bedload flux, with a low transport activity between January and April, and an extended period of high transport activity between June and December. The monthly-averaged bedload rating curve of the Moulin obtained for the 1990-2019 period clearly illustrates the shifting bedload response occurring after September, with a strong anticlockwise hysteresis pattern (Fig. 7), as observed with the event-based dataset.

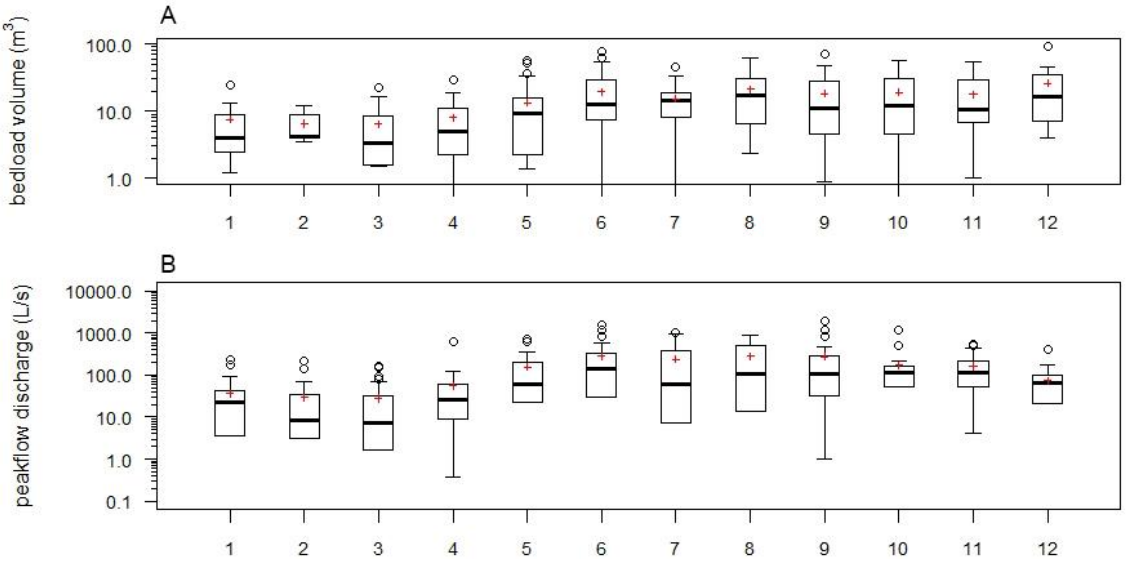

Figure 6. Monthly box plots of (A) bedload transport volumes and (B) peak water discharges for the 1990-2019 period in the Moulin; red crosses correspond to monthly means.

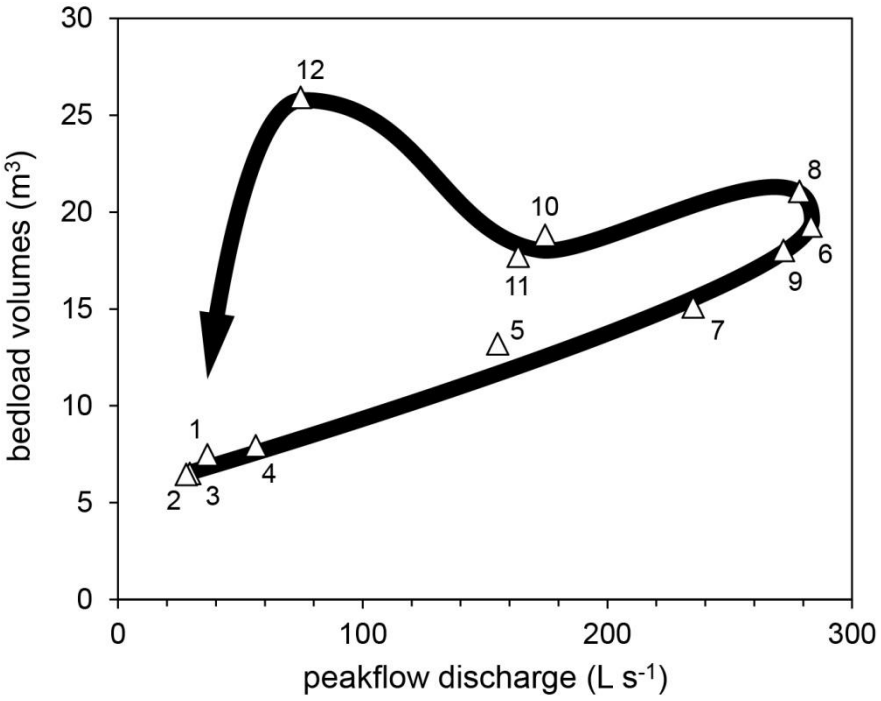

Figure 7. The variation of monthly-averaged bedload volumes with monthly-averaged peak water discharges for the 1990-2019 period in the Moulin, showing an anticlockwise seasonal hysteresis; numbers correspond to months.

4.2. High-frequency bedload response to flow

Between autumn 2011 and spring 2018, the slot sampler was operational during 39 flow events relatively well distributed throughout the seasons (24 events during spring-summer, and 15 during autumn-winter). Bedload recording is composed of 843 one-minute bedload fluxes, ranging from 0.07 to 23.43 kg m^{-1} s^{-1}, and covering a large shear stress spectrum (3 - 134 N m^{-2}, corresponding to Shields numbers in the range 0.09 - 2.12; Shields number computed with the D_{50} of the bedload collected in the slot sampler). The maximum recorded bedload flux was obtained during the June 6, 2013 convective storm, with a high (1,592 L s^{-1}) peak water discharge. This event is the largest in record since the deployment of the slot sampler, and the second largest in record since the onset of hydrological monitoring in the Moulin (Fig. 4).

Each recorded flow event was classified with respect to the channel phase by considering the time evolution of the alluvial storage based on scour-chain surveys (Fig. 8). These surveys reveal fairly

regular seasonal cycles of channel cut-and-fill, with aggradation during spring and summer, and degradation during autumn and winter. Amplitudes of the seasonal cycles were particularly strong between 2011 and 2015, and they were dampened after 2015, due to a lower hydrological activity. Bedload recording shows a prevalence of data for equilibrium conditions (43%), with aggradation and degradation conditions representing 32% and 25% of the dataset, respectively.

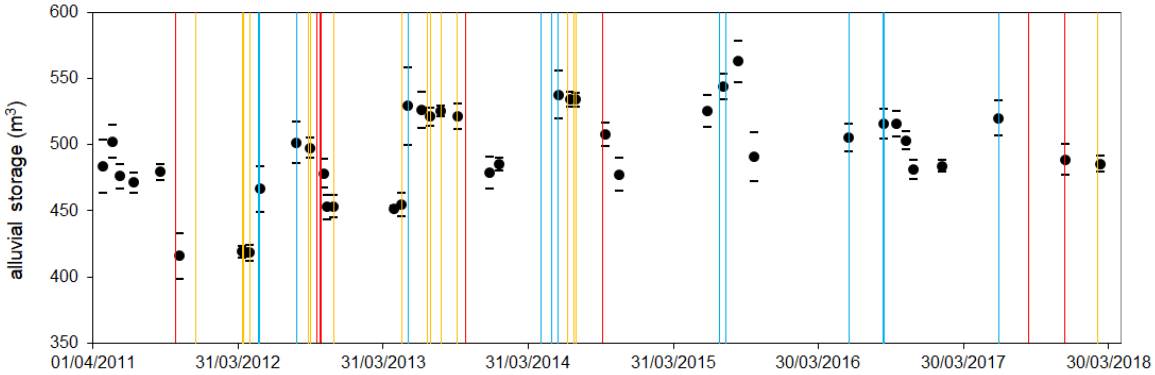

Figure 8. Classification of bedload transport monitoring events in three channel phases according to the time-evolution of the alluvial storage obtained from scour-chain surveys: aggradation events in blue, degradation events in red, equilibrium events in yellow; error bars of alluvial storage volumes are derived from standard errors of mean scour and fill.

Bedload rating curves using shear stress have been extracted for each channel phase (Fig. 9). Although the data are scattered, typical of field-based bedload datasets, a clear gradient between channel phases emerges, with a much more intense bedload transport (for a given shear stress) during degradation as compared to aggradation. The bedload response of the equilibrium phase is approximately in between the two other groups. This gradient reflects a seasonal anticlockwise hysteresis of bedload response, as aggradation prevails during spring and summer, and degradation prevails during autumn and spring. Power laws offer the best fits to the data, with R^2 of 0.75, 0.73, and 0.54 for degradation, equilibrium, and aggradation conditions, respectively (Table 2). Equivalent figures using linear regression models are 0.71, 0.54, and 0.40 for degradation, equilibrium and aggradation, respectively. Exponents of power laws for aggradation and degradation are fairly similar, with values close to 1.3, while a significantly higher exponent is obtained for equilibrium conditions (around 1.6). An ANCOVA was

429 performed to test for the effect of the channel phase on bedload transport, with only two groups:
430 aggradation and degradation. Results show very significant differences in intercepts of regression
431 models (F=71.873, p<0.001), and similar slopes (F=0.796, p=0.373). The effect of the channel phase
432 on bedload transport is statistically confirmed, and the rate of bedload transport with discharge is
433 unaffected by phase. The scatterplot shows a remarkable data alignment below an envelope curve
434 joining maximum bedload fluxes for a given shear stress, with a slope equivalent to aggradation and
435 degradation phases. By considering the minimum bedload flux that can be detected by the slot sampler
436 during the monitoring program (0.07 kg m^{-1} s^{-1}), power law fits can be used to evaluate the mean
437 critical shear stress for each channel phase, following the approach proposed in several papers using
438 bedload data from slot samplers (Reid et al., 1998; Cohen et al., 2010). This approach gives values of
439 3.5, 5.5, and 7.1 N m^{-2} for degradation, aggradation, and equilibrium, respectively. However, the fact
440 that the slope of the power law obtained for the equilibrium phase is significantly higher than for the
441 other groups has no obvious reason, and caution is suggested in interpreting this power law.

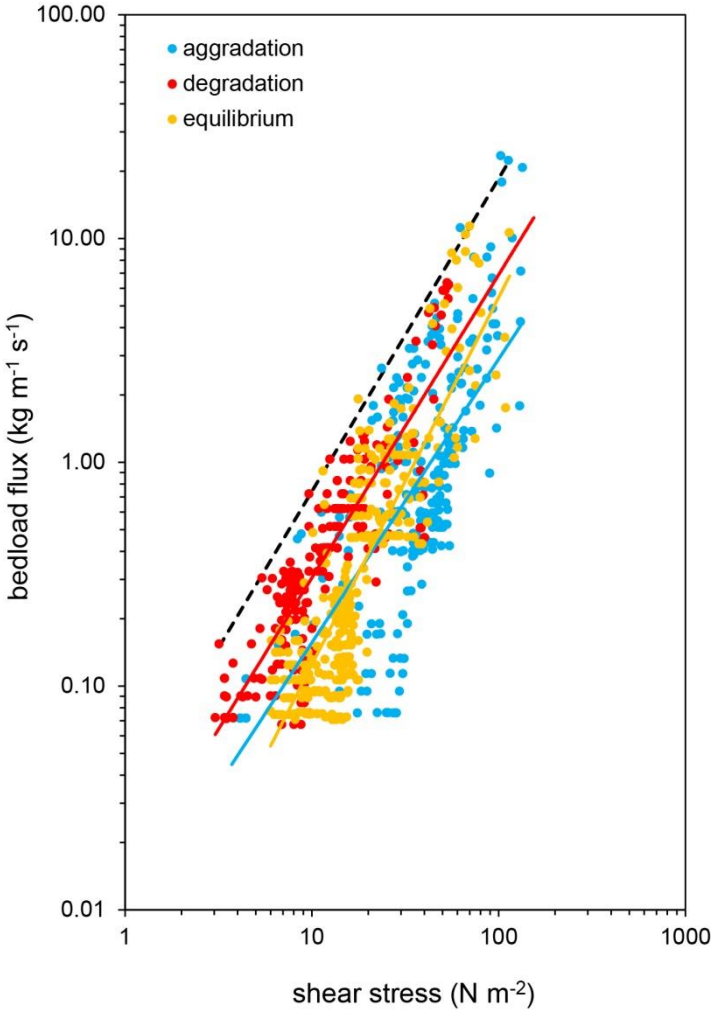

Figure 9. Bedload response to shear stress as a function of the channel phase obtained from the slot-sampler data; the envelope curve in black has been manually fitted.

	Aggradation	Equilibrium	Degradation
Best fit (power law)	$Q_b=0.008\tau^{1.27}$	$Q_b=0.0028\tau^{1.64}$	$Q_b=0.013\tau^{1.35}$
R^2	0.54	0.73	0.75
F Fisher	303.0	1018.0	658.9
p-value	<0.0001	<0.0001	<0.0001
N	254	373	216
Constant term (95% CI)	0.005-0.014	0.002-0.004	0.010-0.017
Exponent (95% CI)	1.12-1.41	1.54-1.77	1.25-1.46

Table 2. Summary statistics of linear regressions on log-transformed values of high-frequency bedload flux and shear stress using data from the slot sampler; Q_b: bedload flux (kg m^{-1} s^{-1}); τ: shear stress (N m^{-2}).

5. Discussion

The long-term record of time-integrated bedload yields of the Moulin, as well as the short-term record of bedload fluxes with a slot sampler both reveal a strong seasonal effect on bedload response to flow conditions. A counterclockwise seasonal hysteresis is observed with the two datasets, showing an increase of bedload transport rate through the year. Most of the reported seasonal bedload hysteresis in upland catchments are generally of clockwise type, under the effect of the early flushing of the readily available sediment mass (e.g. Nanson, 1974; Moog and Whiting, 1998; Pearce et al., 2003; Yu et al., 2009; Schneider et al., 2016; Rickenmann, 2018; Misset et al., 2020). One case of counterclockwise hysteresis at the seasonal timescale has been reported in a proglacial river of the Italian Alps, which has been attributed to the delayed sediment supply from glacial and proglacial zones of the catchment (Comiti et al., 2019).

The singular seasonal signature of bedload transport in the Moulin can be closely linked with a yearly travelling sediment pulse inferred from regular seasonal cycles of cut-an-fill along the main alluvial branches of the catchment. The lower bedload transport efficiency during spring and early summer can be interpreted as a consequence of aggrading channel conditions during this time of the year. This aggrading phase is explained by the entrainment and transient storage of loose debris produced by frost cracking on hillslopes during winter. When the channel is aggrading, most of the coarse sediment load is temporary stored along the main channel, and supply-limited conditions prevail at the catchment outlet. A lower bedload transport efficiency is, therefore, observed during spring and summer, while those seasons correspond to the most active hydrological period of the year. Highest peak water discharges in the Moulin are related to convective storms occurring during late spring and summer. Once the aggrading phase has ended, a new confined and narrow channel forms in the alluvial fill by incision and lateral shifting, subsequently transferring the yearly sediment pulse downstream. The high bedload activity observed during autumn and early winter can, hence, be regarded as the delayed propagation of a sediment wave. Even in a catchment as small and as steep as the Moulin, it appears that the direct transfer of sediment from hillslopes to the catchment outlet during a flow event is quite uncommon. This is likely the case for some of the documented summer

flow events in aggradation phase, showing a bedload response equivalent to the degradation group (Fig. 9). However, mean bedload responses of phases of aggradation and degradation clearly suggest a strong control of the alluvial system in the export of bedload from the catchment. This type of control was also observed in a small siltstone badland catchment in Wyoming (Bergstrom, 1982).

Direct evidence of the effect of travelling sediment pulses on bedload transport has been restricted to flume experiments (Hoey and Sutherland, 1991; Lisle et al., 1997; Cui et al., 2003). The intensive and coincident monitoring of bedload transport and channel storage change of the Moulin provides a direct field validation of the importance of travelling sediment pulses for the prediction of bedload response to flow. This has some implications for the modelling of bedload transport, notably in small mountain streams where sediment waves are regularly released from erosion processes on hillslopes. Bedload transport modelling should, therefore, go beyond a local-scale mechanistic approach based on reach-scale hydraulic and morpho-sedimentary conditions, and should more fully integrate catchment-scale sediment cascading effects (Schmitt et al., 2016). Of particular importance would be to integrate advances in sediment wave modelling along the stream network (Gran and Czuba, 2017), and memory effects of antecedent flow events, which may substantially improve the prediction of bedload transport, as recently demonstrated in the Erlenbach torrent through cyclic fluctuations of the disequilibrium ratio between bedload transport and transport capacity derived from a bedload transport equation (Rickenmann, 2020).

Field observations at the Moulin have also direct implications for bedload transfer in temperate upland catchments with a strong geomorphic connectivity between hillslopes and the stream network. Under such conditions, the sediment cascade is supplied every year by loose debris produced during the cold season, due to frost-cracking processes on bedrock (Ariagno et al., in press). This weathering process is particularly active in the Moulin, due to specific geological conditions (marls highly sensitive to frost-cracking). The interplay of this weathering cycle and the rainfall regime controls the initiation and transfer of sediment pulses, and subsequently the counterclockwise seasonal hysteresis of catchment bedload yield. It should, therefore, be considered that the inter-annual variability of the

bedload yield in such catchments should be not only controlled by the hydrology, but also by the weathering intensity during the cold season, which depends on the frost-cracking windows (Walder and Hallet, 1985; Hales and Roering, 2005). The long-term bedload monitoring program of the Draix observatory provides a quasi-unique dataset to look more closely at these climatic controls on bedload dynamics, at different spatial scales (4 catchments are equipped with a sediment trap until the 1980s, see Mathys et al, 2003). More research should be done to investigate this question.

To what extent can the bedload response of the Moulin be generalized to small alpine headwaters? Annual sediment pulses are likely common in most of the alpine headwaters with active gully erosion on hillslopes. This has already been documented in a rocky sandstone debris-flow initiation zone in Japan (Imaizumi et al., 2006) and in a small debris-flow catchment of the Northern French Prealps with active gully erosion in alternating sequences of marls and limestones (Theule et al., 2012; Loye et al., 2016). In this catchment, regular laser scanning of the rocky sediment production zone clearly documented an intensive production of loose debris by frost-cracking during winter (Loye et al., 2016). Gully erosion activated during the first spring runoff easily remobilizes the loose debris, which accumulates during winter as scree-mantled slopes or debris-fans in the sides of headwater channels. In the marly badlands of the Moulin, dry ravel seems to be a key process for the formation of these colluvial deposits (personal observations from the authors). When a strong sediment connectivity exists between upstream active gully erosion zones and the alluvial system downstream, yearly sediment pulses can easily propagate through the stream network. These annual sediment pulses are likely not present in small alpine catchments with stable vegetated hillslopes, or in catchments with strong sediment disconnectivity between exposed bedrock outcrops and the alluvial system. These pulses are also likely rapidly dampening downstream under the effect of sediment wave dispersion.

6. Conclusion

The long-term monitoring of time-integrated bedload yields of the Moulin marly badland catchment showed a seasonal counterclockwise hysteresis of bedload response to flow conditions. Autumn and early winter flow events transport on average more bedload than spring and summer events, despite

peak water discharges being much more intense during the warm seasons, under the effect of convective storms. This behavior is confirmed by high-frequency bedload fluxes captured with a slot sampler, which have been monitored concomitantly with alluvial storage changes in the channel upstream of the slot sampler. It is shown that bedload fluxes are significantly higher during periods of channel degradation, which systematically occur during autumn and early winter. The seasonal counterclockwise bedload hysteresis can be therefore attributed to a yearly sediment pulse reaching the catchment outlet during the peak of the degradation phase. We suggest that these seasonal bedload pulses are likely typical of small alpine catchments with active gully erosion into bedrock sensitive to frost-cracking.

Declaration of competing interest

The authors declare that they have no known competing financial interests or personal relationships that could have appeared to influence the work reported in this paper.

Acknowledgements

This study was undertaken in the framework of the long-term erosion observatory of Draix-Bléone. It was supported by OSUG, Univ. Grenoble Alpes, and the French ANR project SegSed (ANR16-CE01-0005). The Draix-Bléone Observatory is funded by INRAE, CNRS-INSU, and OSUG and is part of the French network of Critical Zone Observatories OZCAR, which is supported by the French Ministry of Research, French research institutions and universities. Xavier Ravanat (INRAE Grenoble) and Fred Ousset (INRAE Grenoble) are acknowledged for the support in the design, construction, and deployment of the slot sampler. The support of many people involved in field surveys is acknowledged: Michaël Deschâtres, Julie Favario, Thomas Gagneux, Pascal Humbert, Hugo Jantzi, Louri Leclech, Tristan Machado, Ludovic Michel, Robin Paya, Lucie Pheulpin, Eva Ripert, Ana Lucia Vela. We acknowledge the thorough reviews by Dieter Rickenmann, Francesco Comiti and an anonymous reviewer.

Appendix A. Supplementary data

Supplementary data associated with this article can be found in the online version. These data include spreadsheets of bedload transport databases obtained with the sediment trap and the slot sampler of the Moulin catchment.

References

Aigner, J., Kreisler, A., Rindler, R., Hauer, C. and Habersack, H., 2017. Bedload pulses in a hydropower affected alpine gravel bed river. Geomorphology, 291: 116-127. http://dx.doi.org/10.1016/j.geomorph.2016.05.015

Ariagno, C., Le Bouteiller, C., van der Beek, P. and Klotz, S., in press. Sediment export in marly badland catchments modulated by frost-cracking intensity, Draix-Bléone Critical Zone Observatory, SE France. Earth Surface Dynamics, https://doi.org/10.5194/esurf-2021-49

Barzilai, R., Laronne, J.B. and Reid, I., 2013. Effect of changes in fine-grained matrix on bedload sediment transport in a gravel-bed river. Earth Surface Processes and Landforms, 38(5): 441-448. http://dx.doi.org/10.1002/esp.3288

Benda, L. and Dunne, T., 1997. Stochastic forcing of sediment routing and storage in channel networks. Water Resources Research, 33(12): 2865-2880. https://doi.org/10.1029/97WR02387

Bergstrom, F.W., 1982. Episodic behavior in badlands: its effects on channel morphology and sediment yields. In: F.W. Swanson, R.J. Janda, T. Dunne and D.N. Swanston (Editors), Sediment budgets and routing in forested drainage basins. USDA Forest Service, General Technical Report, PNW-141, pp. 59-66.

Cohen, H., Laronne, J.B. and Reid, I., 2010. Simplicity and complexity of bed load response during flash floods in a gravel bed ephemeral river: a 10 year field study. Water Resources Research, 46(11): W11542. https://doi.org/10.1029/2010WR009160

Comiti, F., Mao, L., Penna, D., Dell'Agnese, A., Engel, M., Rathburn, S. and Cavalli, M., 2019. Glacier melt runoff controls bedload transport in Alpine catchments. Earth and Planetary Science Letters, 520: 77-86. https://doi.org/10.1016/j.epsl.2019.05.031

589 Cui, Y., Parker, G., Lisle, T.E., Gott, J., Hansler-Ball, M.E., Pizzuto, J.E., Allmendinger, N.E. and
590 Reed, J.M., 2003. Sediment pulses in mountain rivers: 1. Experiments. Water Resources Research,
591 39(9): 1239-1250. https://doi.org/10.1029/2002WR001803

592 D'Agostino, V. and Lenzi, M.A., 1999. Bedload transport in the instrumented catchment of the Rio
593 Cordon. Part II : analysis of the bedload rate. Catena, 36: 191-204. https://doi.org/10.1016/S0341-
594 8162(99)00017-X

595 Froehlich, W., 2003. Monitoring bed load transport using acoustic and magnetic devices. In: J. Bogen,
596 T. Fergus and D.E. Walling (Editors), Erosion and Sediment Transport Measurement in Rivers:
597 Technological and Methodological Advances. IAHS Publication 283, Wallingford, pp. 201-210.

598 Fuller, I.C. and Marden, M., 2010. Rapid channel response to variability in sediment supply: cutting
599 and filling of the Tarndale Fan, Waipaoa catchment, New Zealand. Marine Geology, 270(1-4): 45-54.
600 https://doi.org/10.1016/j.margeo.2009.10.004

601 Garcia, C., Laronne, J.B. and Sala, M., 2000. Continuous monitoring of bedload flux in a mountain
602 gravel-bed river. Geomorphology, 34: 23-31. https://doi.org/10.1016/S0169-555X(99)00128-2

603 Gomez, B. and Church, M., 1989. An assessment of bedload sediment transport formulae for gravel
604 bed rivers. Water Resources Research, 25(6): 1161-1186. https://doi.org/10.1029/WR025i006p01161

605 Gomez, B., Naff, R.L. and Hubbell, D.W., 1989. Temporal variations in bedload transport rates
606 associated with the migration of bedforms. Earth Surface Processes and Landforms, 14(2): 135-156.
607 https://doi.org/10.1002/esp.3290140205

608 Gran, K.B. and Czuba, J.A., 2017. Sediment pulse evolution and the role of network structure.
609 Geomorphology, 277: 17-30. http://dx.doi.org/10.1016/j.geomorph.2015.12.015

610 Hales, T.C. and Roering, J.J., 2005. Climate-controlled variations in scree production, Southern Alps,
611 New Zealand. Geological Society of America Bulletin, 33(9): 701-704.
612 https://doi.org/10.1130/G21528.1

613 Hassan, M.A. and Church, M., 2001. Sensitivity of bed load transport in Harris Creek: Seasonal and
614 spatial variation over a cobble-gravel bar. Water Resources Research, 37(3): 813-825.
615 https://doi.org/10.1029/2000WR900346

616 Hoey, T.B., 1992. Temporal variations in bedload transport rates and sediment storage in gravel-bed
617 rivers. Progress in Physical Geography, 16(3): 319-338.
618 https://doi.org/10.1177/2F030913339201600303

619 Hoey, T.B. and Sutherland, A.J., 1991. Channel morphology and bedload pulses in braided rivers: a
620 laboratory study. Earth Surface Processes and Landforms, 16(5): 447-462.
621 https://doi.org/10.1002/esp.3290160506

622 Hsu, L., Finnegan, N.J. and Brodsky, E.E., 2011. A seismic signature of river bedload transport during
623 storm events. Geophysical Research Letters, 38(13). https://doi.org/10.1029/2011GL047759

624 Imaizumi, F., Sidle, R.C., Tsuchiya, S. and Ohsaka, O., 2006. Hydrogeomorphic processes in a steep
625 debris flow initiation zone. Geophysical Research Letters, 33(10).
626 https://doi.org/10.1029/2006GL026250

627 Jackson, W.L. and Beschta, R.L., 1982. A model of two-phase bedload transport in an Oregon Coast
628 Range stream. Earth Surface Processes and Landforms, 7: 517-527.
629 https://doi.org/10.1002/esp.3290070602

630 Jantzi, H., Liébault, F. and Klotz, S., 2017. Sediment residence time in alluvial storage of black marl
631 badlands. Catena, 156: 82-91. https://doi.org/10.1016/j.catena.2017.03.026

632 Klingeman, P.C. and Emmett, W.W., 1982. Gravel bedload transport processes. In: R.D. Hey, J.C.
633 Bathurst and C.R. Thorne (Editors), Gravel-bed Rivers. John Wiley and Sons, Chichester, pp. 141-
634 169.

635 Krein, A., Schenkluhn, R., Kurtenbach, A., Bierl, R. and Barrière, J., 2016. Listen to the sound of
636 moving sediment in a small gravel-bed river. International Journal of Sediment Research, 31(3): 271-
637 278. https://doi.org/10.1016/j.ijsrc.2016.04.003

638 Kuhnle, R.A., 1992. Bedload transport during rising and falling stages on two small streams. Earth
639 Surface Processes and Landforms, 17: 191-197. https://doi.org/10.1002/esp.3290170206

640 Lane, S.N., Richards, K.S. and Chandler, J.H., 1996. Discharge and sediment supply controls on
641 erosion and deposition in a dynamic alluvial channel. Geomorphology, 15: 1-15.
642 https://doi.org/10.1016/0169-555X(95)00113-J

643 Laronne, J.B., Alexandrov, Y., Bergman, N., Cohen, H., Garcia, C., Habersack, H., Powell, D.M. and
644 Reid, I., 2003. The continuous monitoring of bedload flux in various fluvial environments. In: J.
645 Bogen, T. Fergus and D.E. Walling (Editors), Erosion and Sediment Transport Measurement in
646 Rivers: Technological and Methodological Advances. IAHS Publication 283, Wallingford, pp. 134-
647 145.

648 Lenzi, M.A., Mao, L. and Comiti, F., 2004. Magnitude-frequency analysis of bed load data in an
649 Alpine boulder bed stream. Water Resources Research, 40(7). https://doi.org/10.1029/2003WR002961

650 Leopold, L.B., Emmett, W.W. and Myrick, R.M., 1966. Channel and hillslope processes in a semiarid
651 area, New Mexico. US Geological Survey Professional Paper, 352-G: 193-253.

652 Liébault, F., 2017. Geomorphology and sediment transport of alpine fluvial systems: from steep-slope
653 torrents to piedmont gravel-bed rivers. Unpublished Habilitation Thesis (HDR), Université Grenoble
654 Alpes, 150 pp.

655 Liébault, F. and Laronne, J.B., 2008. Evaluation of bedload yield in gravel-bed rivers using scour
656 chains and painted tracers: the case of the Esconavette Torrent (Southern French Prealps).
657 Geodinamica Acta, 21(1-2): 23-34. https://doi.org/10.3166/ga.21.23-34

658 Liébault, F., Jantzi, H., Klotz, S., Laronne, J.B. and Recking, A., 2016. Bedload monitoring under
659 conditions of ultra-high suspended sediment concentrations. Journal of Hydrology, 540: 947-958.
660 http://dx.doi.org/10.1016/j.jhydrol.2016.07.014

661 Liébault, F., Klotz, S., Jantzi, H. and Ravanat, X., 2017. Monitoring du charriage avec une trappe à
662 fente, observatoire de Draix. Collection EDYTEM, 19: 221-226.

Lisle, T.E., Pizzuto, J.E., Ikeda, H., Iseya, F. and Kodama, Y., 1997. Evolution of a sediment wave in an experimental channel. Water Resources Research, 33(8): 1971-1981. https://doi.org/10.1029/97WR01180

Loye, A., Jaboyedoff, M., Theule, J.I. and Liébault, F., 2016. Headwater sediment dynamics in a debris flow catchment constrained by high-resolution topographic surveys. Earth Surface Dynamics, 4(2): 489-513. https://doi.org/10.5194/esurf-4-489-2016

Mao, L., Dell'Agnese, A., Huincache, C., Penna, D., Engel, M., Niedrist, G. and Comiti, F., 2014. Bedload hysteresis in a glacier-fed mountain river. Earth Surface Processes and Landforms, 39(7): 964-976. http://dx.doi.org/10.1002/esp.3563

Mao, L., 2018. The effects of flood history on sediment transport in gravel-bed rivers. Geomorphology, 322: 196-205. https://doi.org/10.1016/j.geomorph.2018.08.046

Mathys, N., Brochot, S., Meunier, M. and Richard, D., 2003. Erosion quantification in the small marly experimental catchments of Draix (Alpes de Haute Provence, France), calibration of the ETC rainfall-runoff-erosion model. Catena, 50(2-4): 527-548. https://doi.org/10.1016/S0341-8162(02)00122-4

Mathys, N., 2006. Analyse et modélisation à différentes échelles des mécanismes d'érosion et de transport de matériaux solides: cas des petits bassins versants de montagne sur marne (Draix, Alpes-de-Haute-Provence). Unpublished PhD Thesis, Institut National Polytechnique de Grenoble, 306 pp.

Meade, R. H., Emmett, W.W., and Myrick, R.M., 1981. Movement and storage of bed material during 1979 in East Fork River, Wyoming, USA. International Association of Hydrological Sciences Publication 132, 225-235.

Meirovich, L., Laronne, J.B. and Reid, I., 1998. The variation of water-surface slope and its significance for bedload transport during floods in gravel-bed streams. Journal of Hydraulic Research, 36(2): 147-157. https://doi.org/10.1080/00221689809498630

Milhous, R.T., 1973. Sediment transport in a gravel-bottomed stream. Unpublished PhD Thesis, Oregon State University, 248 pp.

Misset, C., Recking, A., Legout, C., Bakker, M., Bodereau, N., Borgniet, L., Cassel, M., Geay, T., Gimbert, F., Navratil, O., Piégay, H., Valsangkar, N., Cazilhac, M., Poirel, A. and Zanker, S., 2020. Combining multi-physical measurements to quantify bedload transport and morphodynamics interactions in an Alpine braiding river reach. Geomorphology, 351: 106877. https://doi.org/10.1016/j.geomorph.2019.106877

Monteith, H. and Pender, G., 2005. Flume investigations into the influence of shear stress history on a graded sediment bed. Water Resources Research, 41(12). https://doi.org/10.1029/2005WR004297

Moog, D.B. and Whiting, P.J., 1998. Annual hysteresis in bed load rating curves. Water Resources Research, 34(9): 2393-2399. https://doi.org/10.1029/98WR01658

Nanson G.C. 1974. Bedload and suspended-load transport in a small, steep mountain stream. American Journal of Science, 274: 471-486. https://doi.org/10.2475/ajs.274.5.471

Nicholas, A.P., Ashworth, P.J., Kirkby, M.J., Macklin, M.G. and Murray, T., 1995. Sediment slugs: large scale fluctuations in fluvial sediment transport rates and storage volumes. Progress in Physical Geography, 19(4): 500-519. https://doi.org/10.1177/2F030913339501900404

Pearce, J.T., Pazzaglia, F.J., Evenson, E.B., Lawson, D.E., Alley, R.B., Germanoski, D. and Denner, J.D., 2003. Bedload component of glacially discharged sediment: Insights from the Matanuska Glacier, Alaska. Geology, 31(1). https://doi.org/10.1130/0091-7613(2003)031%3C0007:BCOGDS%3E2.0.CO;2

Phillips, B.C. and Sutherland, A.J., 1990. Temporal lag effect in bed load sediment transport. Journal of Hydraulic Research, 28(1): 5-23. https://doi.org/10.1080/00221689009499144

Piton, G. and Recking, A., 2017. The concept of travelling bedload and its consequences for bedload computation in mountain streams. Earth Surface Processes and Landforms, 42(10): 1505-1519. https://doi.org/10.1002/esp.4105

Poreh, M., Sagiv, A. and Seginer, I., 1970. Sediment sampling efficiency of slots. Journal of Hydraulics Division, 96(10): 2065-2078. https://doi.org/10.1061/JYCEAJ.0002729

713 Recking, A., Frey, P., Paquier, A. and Belleudy, P., 2009. An experimental investigation of
714 mechanisms involved in bed load sheet production and migration. Journal of Geophysical Research,
715 114. F03010, https://doi.org/10.1029/2008JF000990

716 Reid, I., Layman, J.T. and Frostick, L.E., 1980. The continuous measurement of bedload discharge.
717 Journal of Hydraulic Research, 18(3): 243-249. https://doi.org/10.1080/00221688009499550

718 Reid, I., Frostick, L.E. and Layman, J.T., 1985. The incidence and nature of bedload transport during
719 flood flows in coarse-grained alluvial channels. Earth Surface Processes and Landforms, 10: 33-44.
720 https://doi.org/10.1002/esp.3290100107

721 Reid, I., Laronne, J.B. and Powell, D.M., 1998. Flash-flood and bedload dynamics of desert gravel-
722 bed streams. Hydrological Processes (12): 543-557. https://doi.org/10.1002/(SICI)1099-
723 1085(19980330)12:4%3C543::AID-HYP593%3E3.0.CO;2-C

724 Rickenmann, D., 1997. Sediment transport in Swiss torrents. Earth Surface Processes and Landforms,
725 22: 937-951. https://doi.org/10.1002/(SICI)1096-9837(199710)22:10%3C937::AID-
726 ESP786%3E3.0.CO;2-R

727 Rickenmann, D., 2018. Variability of bed load transport during six summers of continuous
728 measurements in two Austrian mountain streams (Fischbach and Ruetz). Water Resources Research,
729 54(1): 107-131. https://doi.org/10.1002/2017WR021376

730 Rickenmann, D., 2020. Effect of sediment supply on cyclic fluctuations of the disequilibrium ratio and
731 threshold transport discharge, inferred from bedload transport measurements over 27 years at the
732 Swiss Erlenbach Stream. Water Resources Research, 56(11): e2020WR027741.
733 https://doi.org/10.1029/2020WR027741

734 Roth, D.L., Finnegan, N.J., Brodsky, E.E., Cook, K.L., Stark, C.P. and Wang, H.W., 2014. Migration
735 of a coarse fluvial sediment pulse detected by hysteresis in bedload generated seismic waves. Earth
736 and Planetary Science Letters, 404: 144-153. https://doi.org/10.1016/j.epsl.2014.07.019

737 Ryan, S.E., Porth, L.S. and Troendle, C.A., 2005. Coarse sediment transport in mountain streams in
738 Colorado and Wyoming, USA. Earth Surface Processes and Landforms, 30: 269-288.
739 https://doi.org/10.1002/esp.1128

740 Schmitt, R.J.P., Bizzi, S. and Castelletti, A., 2016. Tracking multiple sediment cascades at the river
741 network scale identifies controls and emerging patterns of sediment connectivity. Water Resources
742 Research, 52(5): 3941-3965. https://doi.org/10.1002/2015WR018097

743 Schneider, J.M., Rickenmann, D., Turowski, J.M., Schmid, B. and Kirchner, J.W., 2016. Bed load
744 transport in a very steep mountain stream (Riedbach, Switzerland): Measurement and prediction.
745 Water Resources Research, 52(12): 9522-9541. https://doi.org/10.1002/2016WR019308

746 Sidle, R.C., 1988. Bed load transport regime of a small forest stream. Water Resources Research,
747 24(2): 207-218. https://doi.org/10.1029/WR024i002p00207

748 Theule, J.I., Liébault, F., Loye, A., Laigle, D. and Jaboyedoff, M., 2012. Sediment budget monitoring
749 of debris-flow and bedload transport in the Manival Torrent, SE France. Natural Hazards and Earth
750 System Science, 12(3): 731-749. https://doi.org/10.5194/nhess-12-731-2012

751 Vatne, G., Takøy Naas, O., Skårholen, T., Beylich, Å. and Berthling, I., 2008. Bed load transport in a
752 steep snowmelt-dominated mountain stream as inferred from impact sensors. Norwegian Journal of
753 Geography, 62(2): 66-74. https://doi.org/10.1080/00291950802094817

754 Walder, J. and Hallet, B., 1985. A theoretical model of the fracture of rock during freezing. Geological
755 Society of America Bulletin, 96(3): 336-346. https://doi.org/10.1130/0016-
756 7606(1985)96%3C336:ATMOTF%3E2.0.CO;2

757 Warburton, J., 1992. Observations of bed load transport and channel bed changes in a proglacial
758 mountain stream. Arctic and Alpine Research, 24(3): 195-203.
759 https://doi.org/10.1080/00040851.1992.12002946

760 Whiting, P.J., Stamm, J.F., Moog, D.B. and Orndorff, R.L., 1999. Sediment-transporting flows in
761 headwater streams. Geological Society of America Bulletin, 111(3): 450-466.
762 https://doi.org/10.1130/0016-7606(1999)111%3C0450:STFIHS%3E2.3.CO;2

763 Yu, G.-A., Wang, Z.-Y., Zhang, K., Chang, T.-C. and Liu, H., 2009. Effect of incoming sediment on
764 the transport rate of bed load in mountain streams. International Journal of Sediment Research, 24:
765 260-273. https://doi.org/10.1016/S1001-6279(10)60002-9

766 Zapico, I., Laronne, J.B., Lucía, A. and Martín-Duque, J.F., 2018. Morpho-textural implications to
767 bedload flux and texture in the sand-gravel ephemeral Poveda Gully. Geomorphology, 322: 53-65.
768 https://doi.org/10.1016/j.geomorph.2018.08.02